Iterative Deconvolution of Regional Waveforms and a Double-Event Interpretation of the 2003 Lefkada Earthquake, Greece

by Jiří Zahradník, Anna Serpetsidaki, Efthimios Sokos and G-Akis Tselentis

Abstract The moment tensor inversion for multiple point sources, based on Kikuchi and Kanamori (1991), was extended to full waveform data at regional (or local) distances. The new code proved to be efficient for retrieving major source contributions of the 2003 Lefkada, Greece earthquake. The source model was derived from five 3-component regional stations (epicentral distances < 140 km), at periods 10-20 seconds. Two main events dominated the rupture process, one at the Lefkada Island (comprising three subevents of total moment 0.9e18 Nm) and the other at the Cephalonia Island (comprising one subevent of 0.5e18 Nm). Their spatial and temporal separation is 40 km and 14 seconds, respectively. They can be understood as two earthquakes. The uncertainty estimate based on reduced data sets (repeatedly excluding a station) shows that the Cephalonia subevent, as well as the major Lefkada subevent are very well resolved regarding their position, time and focal mechanism. The source model explains well the aftershock distribution, characterized by two clusters at the Lefkada and Cephalonia Islands, respectively. The focal mechanism of the two main subevents are predominantly right-lateral strike slip of SSW-NNE orientation. The Cephalonia subevent occurred on a less steeply dipping fault, with a small thrust component. Large deviations from pure double couple were found, but interpreted as artifacts. The new software developed in this paper (Fortran code and Matlab graphic user interface) is freely available.

Introduction

The Ionian Islands (e.g. Zakynthos, Cephalonia, Lefkada, Corfu) belong to the most seismically active regions of the Mediterranean. The Cephalonia transform fault, Fig. 1, in the transition between Hellenic subduction to the south, and continental collision to the north, is a major feature, dominated by right-lateral strike-slip motion. The northern part of the Cephalonia transform fault, the so-called Lefkada Fault Segment, following the western coast of Lefkada Island, is striking NNE and dipping E, and its length is about 40 km. At least 15 events of magnitude larger than 6 occurred close to Lefkada since the 17th century, the largest events of the last century being M6.3 on Nov. 27, 1914 and M6.5 on April 22, 1948. For details, see Papazachos and Papazachou, 1997; Louvari et al., 1999; Papadimitriou, 2002, and references therein.

This paper studies the most recent M6 event on Lefkada, the earthquake of August 14, 2003 (at 05:14:54 UT), see Table 1. The main objective is to study the source process, and to explain the specific aftershock pattern, dominated by two spatially separated clusters.

Source inversions seeking for space-time variation of slip on a rectangular fault are often inherently non-unique and require additional constraints (Das and Kostrov, 1990). As the slip is usually concentrated in very few areas of the fault (Somerville et al., 1999), a reasonable strategy is to seek just those areas. Promising methods of that kind are the so-called patch inversion (Valee and Bouchon, 2004), or the iterative deconvolution of multiple point sources (Kikuchi and Kanamori, 1991). The latter has been chosen for this study, since it also enables retrieval of the space-time varying moment tensor. The method inspects a set of pre-defined point source positions, i.e. "slip candidates", distributed along a fault plane, or a line. Since the source inversions have usually worse resolution along dip than along strike (Lavalee and Archuleta, 2003), we study only a linear horizontal array of the potential source positions. For similar philosophy, see, e.g. Kuge (2003) and Frankel (2003).

We extend the Kikuchi and Kanamori (1991) technique from teleseismic to regional or local data. To this goal, we developed a completely new computer code, allowing full wavefield inversion, based on the discrete wavenumber method of Bouchon (1981) and Coutant (1989). A useful part of the code is an interactive graphical tool, with which various constraints can be applied during inversion, such as the first-motion polarity constraint, constraint of the fault dipping direction, constraint of the rupture velocity, etc. Extensive numerical tests of the new code on regional waveforms (< 140 km) of the 2003 Lefkada M6 earthquake were performed with main focus on the uncertainty and resolution. More specifically, we will show that two major subevents of this earthquake (separated nearly 40 km from each other) are very stable and well resolved, but the uncertainty increases when proceeding to additional smaller subevents. Thus only four subevents will be reported. As most tests were performed in parallel with unconstrained (deviatoric) moment tensor and the DC-constrained moment tensor, we were able to clearly detect spurious character of the non-DC (CLVD) components. Therefore, we present only the DC-constrained moment tensors. Finally, we discuss the segmented nature of the mainshock, and suggest its interpretation as two earthquakes.

Location

The mainshock and about 470 aftershocks (Aug. 14 - Aug. 30, 2003) were located using records of the short-period telemetered network of the Patras University (PATNET). The HYPO71PC code of Lee and Valdés (1989) was used in three 1D crustal models, those of Tselentis et al. (1996), Haslinger et al. (1999), and Novotný et al. (2001). The model of Novotný et al. (2001) provided non-realistic shallow depths, accompanied by the largest depth errors, so it is not further discussed. The other two models provided similar location results, but the model by Haslinger et al. (1999) allowed more realistic waveform modeling. Therefore, it was used in this paper both for location and for the waveform modeling. In Fig. 2, the locations are shown for 288 events with at least 5 arrival time readings, rms < 0.4 sec, and erh, erz < 10 km. The mainshock coordinates are listed in Table 2.

Major fault of the studied zone, the Cephalonia transform fault, consists of two parts of a slightly different strike (e.g. Louvari et al. (1999): the Lefkada Fault Segment (LFS) and the Cephalonia Fault Segment (CFS). Figure 2 shows that the aftershocks are separated in two clusters, close to the northern and southern edge of the LFS.

Most epicenters are situated to the east of the fault, at least in the northern cluster, which indicates its eastward dip. However, inferences regarding the dip angle should be avoided. In

fact, as intuitively expected due to the lack of stations west of the epicenter, formal error analysis, based on covariance matrix, showed that the EW error is about 50% larger compared to the NS error. The true foci are probably shifted somewhat to the west, but the absolute value of such a shift remains unknown.

It is to emphasize, that although the two clusters are well separated in space, they operated practically simultaneously. Although it is not easy to identify wave onsets soon after the mainshock, an M4 aftershock occurred undoubtedly at Cephalonia already at 05:23:57, i.e. 9 minutes after the mainshock at Lefkada.

Method

This paper uses the iterative deconvolution of multiple point sources, based on Kikuchi and Kanamori (1991). We inspect a set of pre-defined point source positions along a line. Once a major point source contribution (subevent) is found, the corresponding synthetics are subtracted from data, the residual waveform is inverted for another point source, and so on. As the optimum source position of each subevent is to be also retrieved, the technique is non-linear. However, since the point sources are removed consecutively, one after another, each step has only two parameters (source position and onset time), thus contributing to stability of the inversion. The remaining part, i.e. the deviatoric moment tensor inversion, is linear, but again with a low number of parameters, just 5 tensor components. We have newly encoded this technique to allow full wavefield modeling at regional (and local) distances, based on the discrete wavenumber method of Bouchon (1981) and Coutant (1989).

When seeking the subevents, their moment rate has a pre-defined shape and duration. If shorter than the least studied period, it is formally represented by the delta function (as in this paper). The moment tensors of the subevents are retrieved by minimizing L2 misfit between records and synthetics, solving normal equations. The inverse matrix provides formal variance of the moment tensor components, showing how the individual tensor components are resolved with respect to each other, and/or warning about the ill-conditioned inversion. To get a more useful error estimate, reflecting uncertainties due to crustal structure, several artificially generated data (data subsets) should be studied, and that is our favorite approach.

The optimum subevent position and time are found by a grid search, in which we maximize correlation between observed and synthetic waveforms. For simplicity and speed, we use the correlation coefficient, indirectly obtained during the least squares minimization; see equations (6) and (11) of Kikuchi and Kanamori (1991). The grid search is non-unique. Therefore, following again the referenced paper, we plot the correlation between observed and synthetic waveforms as a 2D function of the source position and time, showing also focal mechanism at all trial subevent positions. Such a graphic tool (see later in Fig. 3) allows an interactive control of the "subevents walk" through space and time. In this way we can apply also various constraints. For example, we may prefer focal mechanisms that agree with first motion polarities, as demonstrated later.

Parallel to the DC-unconstrained moment tensor inversion, we run also DC-constrained inversion, using Lagrange multipliers. We use equations (9a) and (9b) of Kikuchi and Kanamori (1991). The constraint is nonlinear; it is applied iteratively. In the first approximation, the determinant and its partial derivatives are evaluated at the best-DC part of the unconstrained moment tensor. To terminate the iteration process we request the DC

percentage to be between 90% and 100%, and, simultaneously, the correlation not worse than 50% of the correlation value of the non-constrained solution.

Fit between the resulting data and synthetics is measured by the variance reduction, defined as *varred* = 1. - (|*residual*| / |*data*|). Here |.| denotes the L2 norm, i.e. the squared amplitudes, summed up over time, components, and stations; and *residual* = *data* - *synthetics*. If a filter is used, it is assumed that it is applied to both the data and synthetics. Then, *varred* . *100* can be understood as percentage of data power explained by the model. It is useful to calculate *varred* after retrieval of each subevent. As the subevents are consecutively removed, the *varred* increases. It is not easy to a priori set up a threshold value of *varred* at which the calculation should terminate, since *varred* value depend on the size of data set, and also on the maximum frequency under study. That is why we should look not only at *varred* value, but also at its change. As a rule, the first few largest subevents increase the variance reduction very quickly, then the increase becomes slow, and we observe a kind of "convergence", indicating that additional subevents are not needed (cannot be resolved). However, as shown later, a stronger criterion is to be applied when deciding whether to add another subevent, or to stop the inversion. Such a criterion is stability. (By the subevent stability we mean that its position, time and mechanism remain similar when perturbing or reducing the data set.) Unstable subevents cannot be accepted even if they still formally increase *varred* .

Data and Preliminary Tests

Five nearest broad band stations were selected for the waveform modeling (Fig. 1). Four stations (KEK, JAN, EVR, RLS) belong to NOA-IG, i.e. National Observatory of Athens, Institute of Geodynamics. One station (SER) is jointly operated by the Charles University, Prague and the University of Patras. The NOA stations are equipped by Lennartz 20 sec sensors, while SER has Guralp 100 sec sensor. The SER records are available at http://seis30.karlov.mff.cuni.cz.

The velocity records were band passed filtered between 0.05 and 0.1 Hz, instrumentally corrected, and integrated to displacement. The studied time window was 200 sec, starting at the hypocentral time. It may be useful to mention that a few tests in a broader frequency range, 0.05-1.0 Hz, provided very similar results (concerning the position and focal mechanism of the two main subevents). Obviously, with the simple crustal model, the variance reduction was much worse, so hereafter we stay below 0.1 Hz.

The periods 10 to 20 sec, and the relatively small epicentral distances (< 140 km), enable some insight into the source process. At the same time, knowledge of the crustal structure is sufficient at those periods. We proved the latter by successful point-source forward modeling of a M5 aftershock (August 14 at 16:18 UT). The Lefkada mainshock was also subjected to a preliminary single point-source forward modeling, but the agreement with data was very poor, thus indicating importance of the finite source extent.

In our preliminary analysis of the Lefkada earthquake, 9 trial source positions were used, with the spacing of 10 km, distributed along a straight line passing through the epicenter (unpublished report by Zahradník et al., 2003, posted on the EMSC web page, http://www.emsc-csem.org/). Two major source positions were identified, one at Lefkada, and the other at Cephalonia, 40 km from each other. As a next step, a long series of tests was made to check the effect of the varying position of the source line, depth of the source line

and the crustal model. Basically, in the following text we focus only on the robust results, practically independent of these variations. Specifically, as previously mentioned, the inversion reported below is based on the crustal model of Haslinger et al. (1999), and the line of trial sources is situated at the hypocentre depth of 13 km (Table 2).

Another important issue is reliability of the moment tensor inversion regarding its double-couple (DC) part, and the non-DC part, respectively. In all tested cases (hundreds of tests) we found that coming through the regions of the highest 2D correlation of the DC-unconstrained inversion, there were closely spaced solutions whose best-DC mechanisms differed by a few degrees in strike, dip, rake, but their DC percentage varied as much as 40 to 90 %. This common behavior was understood as a strong indication that the non-DC part (CLVD) is an artifact. It should be noted that with a plain least-square inversion, without the correlation analysis, it would be much more difficult to recognize the false non-DC solutions. Moreover, in our data set, the DC-constrained solution is very close to the best-DC part of the unconstrained solution. Specifically, their deviation is much smaller than the deviations introduced by artificially perturbing the data set. At the same time, we found that the DC-constraint has negligible effect (about 1 %) upon the resulting variance reduction. If a non-DC component exists, it cannot be resolved with the available data. For all these reasons, we present only the best-DC part of the DC-constrained solution, not the complete moment tensor.

Results

Subevents 1 and 2

The present study started with the following set-up of the trial source positions: 15 trial source positions were distributed along a straight line at the depth of 13 km, striking N20^{o}E, and passing through the hypocenter (38.84^o N, 20.60^o E). It extended 10 km to the north from the hypocenter, and 60 km to the south, without any gap, and had the 5 km spacing between the trial positions. Ten subevents were formally retrieved. The largest two occurred 10 and 45 km from the hypocenter (towards the south). All the other subevents had their moment smaller than 1/2 of subevent 1 or 2. None of them occurred in the region spanning the interval of 20 to 40 km, measured from the hypocenter towards the south, thus strongly indicating a low slip region there.

Therefore, to make even a more detailed insight into the source process, hereafter we focus onto another set-up along the same line, i.e. 18 trial point-source positions, 9 at Lefkada and 9 in Cephalonia, now with the spacing of 2.5 km (see Fig. 2). We emphasize that the idea to leave the 20-km segment between Lefkada and Cephalonia free of the trial source positions is not based on the knowledge of the aftershock clustering. It is nothing but a "zooming" suggested by the previous calculation with the equidistant positions.

To determine the 1st subevent, we analyze the 2D correlation plot of Fig. 3a. Due to limited resolution at $f < 0.1$ Hz, the correlation is not sharply peaked. Anyway, as in the preliminary test, we have a choice between two main source contributions, characterized by nearly the same amount of correlation; see the smooth maxima smeared between the source positions 1 to 6, and 10 to 13. Note also that the maxima in Fig. 3 are "doubled" along the horizontal time axis, roughly at a half-period distance. This is an undesired consequence of the fact that we work in a relatively narrow frequency band, in which waveforms are close to sinusoidal, so

that a half-period shifted function of the opposite sign fits the data equally well. One of the "double" maxima is false, and could produce a wrong focal mechanism. For example, fix a source position 4, and move along the time axis from the left to the right. You find the major cloud at time ~3 sec, with predominantly right-lateral strike slip, and the other one (with a lower correlation) at time ~10 sec, featuring the left-lateral motion. The latter, however, contradicts the first motion polarities, so we must ignore it. This is how we apply the first-motion polarity constraint. Another, more subtle feature to be mentioned, is the fault dip. The formal global maximum value of the 2D correlation (position 1, time 4 sec) indicates a fault dipping to the west, contradicting the aftershock distribution. However, moving to a slightly lower correlation, we easily find the east-dipping solution (position 4, time 2 sec), and this is our second, weaker constraint, when retrieving the 1st subevent. The final solution for the 1st subevent is in Table 3, and it is also shown by a beach ball in Fig. 2.

Now we calculate the corresponding point-source synthetics of the 1st subevent, remove it from the data, and get a new 2D correlation map (Fig. 3b), representing our starting point for retrieving the 2nd subevent. The formal maximum of correlation at position 12 and time of 16 sec provides the focal mechanism similar to the 1st subevent (Fig. 2 and Table 3); it is predominantly right-lateral strike slip, but less steeply dipping, and with a small thrust component. There is no reason to apply any additional constraint here. It is perhaps useful to mention that the parameters of subevents 1 and 2 are almost independent of their retrieval succession; i.e., we could equally well start with removing a subevent at position 12, and then to automatically obtain the next one at position 4.

Let us also mention that, comparing with the above discussed experiment with the 15 equidistant source positions, the major source contributions are now practically the same. Indeed, with the present step of 2.5 km, subevent 1 is only 2.5 km apart from its position in the previous test, (where the step of 5 km was used), with a corresponding change of the dip and rake by 5^{o} and 2^{o}, respectively. Subevent 2 is completely identical to that one from the 15-position test. Seismic moment and timing of both subevents 1 and 2 are the same as in the 15-position test, too. Independence of the step size (5 or 2.5 km) is related to the relatively long periods (10 to 20 seconds) and the relatively large fault lengths of subevents 1 and 2 (see later in the paragraph on the fault segmentation).

It is useful to demonstrate the waveform contribution of the two main subevents. With subevent 1 only, major late phases remain unexplained, e.g. at SER-NS, JAN-EW, RLS-NS. Also the Z component is too small at SER and JAN, and the variance reduction is only 29 %. The summed subevents 1 and 2 basically remove these problems, and the variance reduction increases to 54 %. Figure 4 illustrates these effects for two stations, SER and JAN.

Partial conclusion is that two subevents (Lefkada and Cephalonia) explain the data better than a single event close to the epicenter (Lefkada), and this result is in a good agreement with the two aftershock clusters.

The two subevents cannot be easily recognized in the non-filtered records. The problem is that at all stations, except RLS and SER, the 2nd subevent arrives within the S-wave group of the 1st subevent. In RLS and SER records, there are indeed several prominent arrivals between the first P onset and the S onset, but it is not possible to unambiguously relate two of them with the 1st and 2nd subevent. That is why figures like that are not presented here.

To estimate uncertainty, we employ 5 reduced data sets, each one generated by removal of 1 of the 5 stations. Procedure like that is suggested by the fact that the weakest point of our method is the 1D crustal model, inherently unable to reflect any variation from one source-station path to the other. Therefore, changes of the solution due to inclusion or omission of a station can easily be large. If they are small, it is a strong indication of a robust result. On the other hand, a drawback is that with few stations we are not able to generate a large artificial data set, to understand the statistical distribution of the parameters, and to quantify the confidence intervals. An alternative strategy might be to build up very large artificial data sets by a more delicate perturbations, e.g. by omitting some samples from the time series. It would produce a statistical distribution of the parameters, but its physical meaning is doubtful (there is no physics behind an omitted sample), and the standard deviation would be very small, e.g. smaller than that obtained by comparing source parameter reports from several agencies. In situation like that, and because we mainly aim at understanding relative robustness of the individual subevents, we prefer the station elimination check.

Before repeatedly inverting the reduced 4-station data sets, we fix the position and time of the first two subevents, found from the 5-station data set (position 4 and 12, time 2 and 16 sec, respectively). Then we retrieve their DC-constrained moment tensors. As seen from Fig. 5, showing the composite plot of all nodal lines, and from Table 3, both subevents 1 and 2 have a very stable (well resolved) focal mechanism. It indicates that the reduced data sets are consistent with the fixed position and time. In other words, the fixing is natural. This was also independently checked by repeating the inversion for the reduced data sets while making the subevent position and time free. Indeed, the positions 4 and 12 were always strongly suggested. The time of 16 sec for subevent 2 was always characterized by a high correlation, and by the right-lateral strike slip. It was automatically obtained as a formal maximum in most of the reduced data sets. However, in two of them (when omitting SER, or KEK), the formal maximum of correlation for subevent 2 occurred at 24 sec, and the preferred mechanism was a left-lateral strike slip.

Table 3 needs a small comment regarding the subevent 1 retrieval, with omission of the SER station, since it has the smallest value of *varred* = 15% only. It may open speculations about specific role of the SER instrument and/or a site effect. Although the SER instrument is indeed different from the other stations, it provides the least likely explanation, because at all stations we study the period range 10 to 20 sec only. The site effect is also not likely since SER station does not exhibit a singular behavior systematically for all earthquakes. For any earthquake we may find a station whose behavior is substantially different from the other stations. It is related in a complex manner to the spatial distribution of the stations with respect to the source and its focal mechanism. The specific feature of the SER record of the 2003 Lefkada earthquake is that SER-NS has the largest amplitude of the entire data set. The next two dominant waveforms are JAN-EW and RLS-NS, see Fig. 8. As such, presence of SER record in the inverted data set has a strong control on the solution, providing the major subevent at position 4 (Lefkada). If the station SER is omitted, the dominant waveforms JAN-EW and RLS-NS take the most important role, and their strong late arrivals tend to push the major subevent into position 12 (Cephalonia), time 24 sec, with a left-lateral strike slip, already mentioned above. The artificial constraint of the subevent succession retrieval, position and time then makes the case of SER omission closer to the other reduced data sets, as seen in Table 3 (the right-lateral strike slip), but the seismic moment and *varred* remain significantly lower. Finally, it is to explain that large amplitudes at SER and JAN come from the positions of these stations on the focal sphere, which are nodal for P waves, but,

simultaneously, they are located on the plane containing the P and T axes, where S waves are strong.

Subevents 3 and 4

Crucial point is whether to stop inversion at this level, or to add some more (weaker) subevents. The answer is conditional: Revealing a few weaker source contributions is possible, but it needs more care. Inherent complication, i.e. inapplicability of the "brute force" automatic approach, is demonstrated in Fig. 6. In that case we adopted subevents 1 and 2 as shown in Table 3, and inverted the residual seismograms for the 3rd and 4th subevent quite automatically, i.e. following the formal correlation maxima, without fixing any position and time. In contrast to subevents 1 and 2, the inversion suggested several source positions, strongly varying from one reduced data set to the other, mainly for subevent 4. Consequently, also the focal mechanisms were unstable, as shown in Fig. 6.

Therefore, we keep in mind that exact position and time of subevents 3 and 4 is unresolved, nevertheless, still we might be interested in some estimation of their focal mechanisms. To that goal we artificially fix the position and time of subevents 3 and 4. First, before fixing the position, we analyze the 5-station data set in more detail. Regarding subevent 3, formal maximum of the correlation suggested its position 9 at time of 4 sec. However, comparing with the neighboring subevent 1 at position 4, spaced by 12.5 km, such a solution would imply a non-realistic rupture speed. Therefore, a constraint must be applied. As a compromise, we adopted a nearby solution providing a reasonable speed, while the correlation was only a bit worse: position 7 and time of 5 sec. Using these parameters for subevent 3, the subevent 4 then gets already its reasonable position 7 and time of 26 sec directly, as suggested by the formal correlation maximum. Therefore, we fix both subevents 3 and 4 at position 7, at time 5 and 26 sec, respectively, and proceed to the reduced datasets. As a result, in Fig. 7 we get a more stable estimate of the focal mechanism than that of Fig. 6. Anyway, compared to subevents 1 and 2, it is obvious that the uncertainty increases. Note also (Table 3) that the variance reduction still grows, but slowly.

A partial conclusion is that subevents 3 and 4 represent later rupture episodes spatially close to subevent 1, with different focal mechanisms. Although the uncertainty is large (mainly for subevent 4), the indication of the spatially non-uniform focal mechanism is strong. The complexity of the rupture process is independently supported also by the other experiments, not presented here, in which all attempts to explain the whole earthquake with an extended model of single (fixed) focal mechanism clearly failed.

Figure 8 compares data with synthetics including the four retrieved subevents. To reflect the uncertainty, the whole family of synthetic seismograms is plotted, corresponding to the inversion of all six data sets of Table 3. Final value of the variation reduction is 70%, or less, depending on the reduced data set. Formal continuation of the inversion process with some five more subevents would still (but very slowly) increase *varred*, but not more than up to about 80%, and the uncertainty would also further grow. In other words, the complete 5-station data set, and a 1D crustal model do not contain a consistent information about more source details. Some tests with further reduced data sets, including as few as 2-3 stations, indicated a possible additional subevent at Cephalonia, as well as one situated to the north of the epicenter at Lefkada. The latter not only partially explained a small aftershock cloud there, but it also improved simulation of the strong late phases at KEK station. However, the

uncertainty was large. Therefore, we terminate the inversion with subevent 4. Nevertheless, we bear in mind a part of data power unexplained, which might indicate an unrevealed amount of slip, and we return to this issue later when discussing the fault size.

Speaking about larger uncertainty of subevent 3 and 4, compared to 1 and 2, it is important to note that subevents 3 and 4 are relatively small. It is documented not only by their moments (Table 3), but also by Fig. 9, corresponding to the 5-station inversion. Indeed, comparing with Fig. 4, where the difference between one and two subevents was large, Figure 9 shows that the difference between two and four subevents is much smaller, although not negligible. At this moment it is to decide whether to conclude that the earthquake can be described by the predominant and best resolved part of the solution, i.e. subevents 1 and 2, or it should be described by (at least) four subevents. Obviously, there is no unique objective answer, since it depends on the adopted point of view. We prefer to present four subevents for two reasons: Presenting only the first two (well resolved) subevents would hide the fact that there exists also a small but less certain additional complexity of the source, not well resolved with the available data. Moreover, presenting only the two largest subevents would too much underestimate the total moment.

The Source Segmentation

Before concluding and releasing results for any further use, e.g. for tectonic interpretation, for the Coulomb stress analysis, for strong-motion simulations, etc., the individual features of the solution should be (at least qualitatively) classified in regard of their robustness.

1. The most robust feature is concentration of the moment release in two source segments (or events). The northern segment, at Lefkada, is represented by subevents 1, 3 and 4, while the southern one, at Cephalonia, is represented by subevent 2, respectively. The whole fault length, measured from the hypocenter (source position 1) up to the most distant subevent 2 is of 45 km. These robust source features are sufficient to basically explain the two major aftershock clouds.
2. Another robust feature is the focal mechanism of subevent 1 and 2. Both can be characterized as predominantly right-lateral strike-slip motion, but they are not identical.
3. The least robust feature is the position, time and focal mechanism of subevent 3 and (mainly) subevent 4.

The term "segment" as used in our source inversion has nothing to do with the geological names, such as the Lefkada Fault Segment (LFS), or the Cephalonia Fault Segment (CFS). According to Fig. 2, both source segments (at Lefkada and Cephalonia) correspond to LFS, not to CFS. However, in this paper, such statement has a merely formal meaning since we do not study geological distinction between LFS and CFS.

The last remaining issue is to discuss possible fault size. First, assume that the Lefkada 2003 earthquake was a single earthquake, with a heterogeneous slip distribution, and the total fault length of 45 km. Considering the 4 subevents together, we get total scalar moment (5-station solution) of 1.4e18 Nm, hence Mw=6.1. This is lower moment than that reported by major agencies (Table 1). Two explanations are possible. Increasing the source depth (to 20-30 km) would increase the moment to about 2e18 Nm, Mw=6.2, closer to the other estimates of Table 1, but it would be less compatible with our location results. An alternative explanation appears to be indicated by the fact that our model did not explain the data completely (the 5th

and higher subevents were not included due to their low reliability). If it means that subevents 1-4 are the main asperities, we can estimate the total earthquake size as follows: Denote by Moa, Aa, and Da the moment, rupture area and the average slip on the asperities, and keep symbols Mo, A, D denoting the corresponding quantities for the whole earthquake. Somerville et al. (1999) suggested empirical relations Aa/A=0.22 and Da/D=2, from which it follows that Moa/Mo=0.44. If the total moment of asperities is that of the 4 subevents, Moa = 1.4e18Nm, we arrive at the whole moment of Mo = 3.2e18 (i.e. Mw = 6.3), in agreement with Table 1. Thus we obtained the moment magnitude Mw ranging between 6.1 and 6.3.

However, whatever of the above moment estimation is true, according to empirical relations of Papazachos and Papazachou (1997), the fault length of 45 km would be too large for a single shallow earthquake in Greece of this magnitude. Therefore, we suggest the double-event interpretation, with the ruptures of the northern source segment at Lefkada Island (subevents 1, 3 and 4) and the southern segment at Cephalonia Island (subevent 2) considered as *two* earthquakes.

Therefore, if the above ideas are then separately applied to the two segments, we get a finite-extent (speculative) model as follows: For the Lefkada segment, represented by subevents 1, 3, and 4, the calculated moment is 0.9e18 Nm. If it is the total moment of the Lefkada asperities, Moa, the entire Lefkada moment is Mo = 2.0e18 Nm. Somerville et al. (1999) then implies A = 164 km^2. Assuming further, for simplicity, that the segment length is roughly twice as large as its width, we arrive at a 18 x 9 km hypothetical model of the Lefkada segment. Analogously, for the Cephalonia segment represented by subevent 2 (Moa = 0.5e18 Nm) we get Mo = 1.1e18 Nm, and A = 110 km^2, which may have a size of 15 x 7.5 km. The estimated fault lengths are in agreement with the observed aftershock distribution. Finally, using the above relation Aa/A=0.22 for 3 asperities at Lefkada, and 1 asperity at Cephalonia, we estimate each asperity size as, approximately, 4x4 km. Although a similar asperity model explained the observed strong-ground motions of the 1999 Athens earthquake (Zahradník and Tselentis, 2002), here it is nothing but a working hypothesis for subsequent studies.

Our next goal is to start from the framework of the source model presented above, simulate rupture of the asperities, and try to understand the strong-ground motions. Study like that needs a separate paper, not only because strong-motion data in Greece are not routinely available on Internet, but also because employment of higher frequencies will require a completely different approach (empirical Green functions).

The segmented rupture of this earthquake (i.e. a multiple event explanation) was quite independently suggested also by Benetatos et al. (2004), based on teleseismic data. Karakostas et al. (2004) made inferences about the Coulomb stress transfer, but considered a single source segment (Lefkada) only. Implicit support of the segmented source comes also from the Harvard CMT analysis, providing the 13.5 sec difference between the centroid time and hypocentral time, which is unusually large for Mw < 6.3.

Speaking about the Harvard solution, it is useful to mention also its non-shear component (DC = 96%, CLVD = 4%). If we consider our 100% DC solutions of the major subevents 1 and 2, and formally sum up their moment tensors, we get a similar non-shear mechanism (DC = 92%). It demonstrates how spurious non-DC mechanisms can appear in relatively long-period studies when complex sources are considered in the point-source approximation.

Conclusions

The moment tensor inversion for multiple point sources, based on Kikuchi and Kanamori (1991), was extended to the full waveform data at regional (or local) distances, using the discrete wavenumber method of Bouchon (1981) and Coutant (1989). The method was newly encoded, and numerous tests resulted in the following methodical messages.

Convergence of the variance reduction is a too weak criterion to stop the inversion process. Additionally, it is to check relative robustness of the subsequent retrieval of the subevents, and to terminate the inversion when the uncertainty is large. The problem of "what is large" is open, because it is not possible to construct any large, physically meaningful artificial data sets providing the parameter distribution and confidence intervals. Therefore, judgement about the termination of the inversion remains subjective.

It is also subjective whether to require stability of all subevent parameters (their position, time, and focal mechanism), or only some of them. Fixing some of the parameters serves a helpful constraint to reveal the remaining ones. Strategy like this is advisable when we try to learn as much as possible from a limited data set. On the other hand, if the method is used as an intermediate step between routine point-source moment tensor inversion, and a detailed finite-extent source analysis, then a more stringent rejection of uncertain features is preferable. For example, leaving only subevents 1 and 2 in this paper, would already provide a reasonable first approximation of a finite-extent source model.

Stopping inversion due to increasing uncertainty leaves some data power unexplained (e.g., in this paper the variance reduction was not larger than 70%). Therefore, before interpreting the results, e.g. comparing with the aftershock distribution, one has to bear in mind that only the major moment release was addressed, so the true source may be larger, and more complex than reflected by the retrieved subevents.

The iterative deconvolution is a dangerous tool for those users who intend to use it mechanically; the code will nearly always provide "some" solution which, however, can be completely misleading. For example, in this paper, if we omit some station(-s), and work less carefully with the 2D correlation, we may erroneously report the left-lateral strike slip, or the non-DC part (CLVD) as large as 50%. On the other hand, for those using the method as a delicate tool, it may be re-warding. They will appreciate that very few parameters are searched simultaneously at each step, hence little suffering from the trade off. They will also like that the method works as a "transparent box", where effects of various constraints can be clearly seen. And, perhaps most importantly, the user may stop inversion after a few first subevents, save the resulting residual waveforms, and continue under different conditions (e.g., with different trial source positions, free or fixed positions, with or without DC-constraint, etc.). Obviously, all these advantages can be fully used when the method is carefully applied to a few selected earthquakes, rather than automatically employed with massive data sets.

The new code proved to be efficient for retrieving some source complexities of the 2003 Lefkada, Greece earthquake. The source model was derived from five 3-component waveform data at regional distances < 140 km, and periods 10-20 seconds. The model is summarized in Table 3. The source process commenced by a weak (“first-motion”) rupture nucleation at the hypocentre, followed after some 2 seconds by the first significant moment release of 0.47e18 Nm at a distance of 7.5 km to the SSW (measured along the trial source line of Fig. 2). Two

smaller rupture episodes of about 0.2e18 Nm occurred nearby (some 7.5 km to the SSW from the first one), still in Lefkada region, with a delay about 3 and 24 seconds, respectively. The three episodes (subevents 1, 3, 4) may represent asperities of the Lefkada source segment. As soon as 14 seconds later, and 37.5 km to the SSW (measured from the first Lefkada subevent), the activity skipped to the Cephalonia source segment, with its major asperity represented by subevent 2, moment release of 0.49 e18 Nm.

According to formal classification (Fig. 2), both these source segments correspond to the same fault, viz LFS, but it is to stress that no geological aspects have been studied in this paper.

The inversion revealed a non-uniform rupture process, not only regarding its space-time development, but also regarding the focal mechanism. Large deviations from pure double-couple mechanism were found, but interpreted as artifacts. The DC-constrained mechanism is predominantly right-lateral strike slip along a steeply dipping fault of the SSW-NNE orientation (except subevent 4), but there is a strong indication that each individual subevent had a different focal mechanism; see Table 3 and Figs. 5 and 7.

The uncertainty estimates, obtained from reduced data sets (repeatedly removing 1 from 5 stations), show that subevents 1 and 2 are much better resolved than subevents 3 and 4. Two viewpoints on the result are possible: (i) We are not sure with exact position and time of subevents 3 and (mainly) 4, but, when artificially fixing their positions and time, we get some estimate of their focal mechanism and moment. Or, (ii), since the exact position and time of subevents 3 and (mainly) 4, are not known, we reject subevents 3 and 4, at all. Most importantly, whatever decision is made, there are still two comparably strong, and highly certain subevents 1 and 2, which, without any doubt, prove the segmented (double-event) nature of the studied earthquake, and well explain the two major aftershock clusters at the Lefkada and Cephalonia Islands.

More details can be obtained with EGF methods, strong motion data, etc., but it was interesting to study in this paper the limited resolution of the mainshock data from the regional broad-band network, because such data are often immediately available.

An interesting task calling for a separate study is the question what physics (e.g. a triggering) was behind the double-event nature of this interesting earthquake. And what are the Coulomb-stress implications of such a segmented earthquake for future events in the Ionian region. In fact, the studied Aug. 14 earthquake was already followed by another nearby event (M5 earthquake on Nov. 16, 2003, 07:22 at Cephalonia, latitude 38.28 N, longitude 20.38 E), and we should ask whether its position might have been better "predictable" when taking into account the double-event nature of the Aug. 14 event.

Remark: The program package developed in connection with this paper is called ISOLA, to emphasize the focus on the Isolated Asperities. The package, consisting of a Fortran code (author J.Z.) and Matlab graphic user interface (author E.S.), is available upon request.

Acknowledgements

The authors thank Dr. George Stavrakakis, the NOA-IG director, for kindly providing the broad-band seismograms. The GMT software of P.Wessel and W. Smith was used. The work was supported by the following Czech research projects: MSM 113200004, GACR 205/03/1047 and by the EC project EVG3-CT-2002-80006 (MAGMA).

References

Benetatos, Ch., A. Kiratzi, Z. Roumelioti, G. Stavrakakis, G. Drakatos, and I. Latoussakis (2004). The 14 August 2003 Lefkada Island (Greece) earthquake: focal mechanisms of the mainshock and of the aftershock sequence, *J. Seismology* (submitted).

Bouchon, M. (1981). A simple method to calculate Green's functions for elastic layered media, *Bull. Seism. Soc. Am.* **71**, 959-971.

Coutant, O. (1989). Program of Numerical Simulation AXITRA, *Research report*, LGIT, Grenoble.

Das, S. and B.V. Kostrov (1990). Inversion for seismic slip rate history and distribution with stabilizing constraints: application o the 1986 Andreanof Islands earthquake, *J. Geophys. Res.* **95**, 6899-6913.

Frankel, A. (2003). Source process of the M7.9 Denali Fault, Alaska, Earthquake: Sub-events, directivity, and scaling of high-frequency ground motion, *EOS Trans. AGU*, **84(46)**, Fall Meet. Suppl., Abstract S11H-03.

Haslinger, F., E. Kissling, J. Ansorge, D. Hatzfeld, E. Papadimitriou, V. Karakostas, K. Makropoulos, H.-G. Kahle, and Y. Peter (1999). 3D crustal structure from local earthquake tomography around the Gulf of Arta (Ionian region, NW Greece), *Tectonophysics* **304** , 201–218.

Karakostas, V. G., E.E. Papadimitriou, and C.B. Papazachos (2004). Properties of the 2003 Lefkada, Ionian Islands, Greece, earthquake seismic sequence and seismicity triggering, *Geophys. Res. Lett.* (submitted).

Kikuchi, M. and H. Kanamori (1991). Inversion of complex body waves – III, *Bull. Seism. Soc. Am.*, **81**, 2335-2350.

Kuge, K. (2003). Source modeling using strong-motion waveforms: Toward automated determination of earthquake fault planes and moment release, *Bull. Seism. Soc. Am.*, **93**, 639-654.

Lavallee, D. and R.J. Archuleta (2003). Stochastic modeling of slip spatial complexities for the 1979 Imperial Valley, California, earthquake, *Geoph. Res. Letters*, **30**, 49-1 - 49-4.

Lee, W. H. K. and C.M. Valdés (1989). Hypo71PC.Toolbox for seismic data acquisition, processing, and analysis. IASPEI & SSA.

Louvari, E., A.A. Kiratzi, and B.C. Papazachos (1999). The Cephalonia Transform Fault and its extension to western Lefkada Island (Greece), *Tectonophysics* **308**, 223–236.

Novotný, O., J. Zahradník, and G-A.Tselentis (2001). North-western Turkey earthquakes and the crustal structure inferred from surface waves observed in the Corinth Gulf, Greece, *Bull. Seism. Soc. Am.* **91**, 875-879.

Papadimitriou, E.E. (2002). Mode of Strong Earthquake Recurrence in the Central Ionian Islands (Greece): Possible triggering due to Coulomb stress changes generated by the occurrence of previous strong shocks, *Bull. Seism. Soc. Am.* **92**, 3293–3308.

Papazachos, B.C. and C.B. Papazachou (1997). *The Earthquakes of Greece* (Ziti Editions, Thessaloniki).

Somerville, P., K. Irikura, R. Graves, S. Sawada, D. Wald, N. Abrahamson, Y. Iwasaki, T. Kagawa, N. Smith, and A. Kowada (1999). Characterizing crustal earthquake slip models for the prediction of strong ground motion, *Seismol. Res. Letters* **70**, 59-80.

Tselentis, G.-A., N.S. Melis, E. Sokos, and K. Papatsimpa (1996). The Egion June 15, 1995 (6.2 ML) earthquake, Western Greece, *Pure Appl. Geophys.* **147**, 83-98.

Vallee, M. and M. Bouchon (2004). Imaging coseismic rupture in far field by slip patches, *Geophys. J. Int.*, in press.

Zahradník, J., and Tselentis, G.-A. (2002). Modeling strong-motion accelerograms by PEXT method, application to the Athens 1999 earthquake. *In:* Proc. of XXVIII Gen. Assembly of the Europ. Seismol. Commission, 1-6 Sep. 2002, Genoa, Italy (CD-ROM).

Faculty of Mathematics and Physics
Charles University in Prague
V Holesovickach 2, 180 00 Prague
Czech Republic
e-mail: jz@karel.troja.mff.cuni.cz
(J.Z.)

Seismological Laboratory
University of Patras
261 10 Rio
Greece
(A.S., G-A.T.)

Institute of Geodynamics
National Observatory of Athens
P.O. Box 20048, 118 10 Athens
Greece
(E.S.)

Table 1

Basic parameters of the August 14, 2003 Lefkada earthquake as reported by several agencies. SED denotes the seismic service of Switzerland.

Agency	Lat. N (deg.)	Lon. E (deg.)	Depth (km)	Moment (10^{18}Nm)	Strike (deg.)	Dip (deg.)	Rake (deg.)
USGS	39.16	20.61	21	2.0	13	84	172
Harvard	38.70	20.67	15	3.0	18	59	-174
MEDNET	38.88	20.62	24	2.6	196	85	-166
SED	39.16	20.61	21	4.1	14	69	174

Table 2

The PATNET location of the mainshock in three crustal models. The last one is used in this paper.

Crustal model	Lat. N (deg.)	Lon. E (deg.)	Depth (km)
Novotný et al. (2001)	38.85	20.65	1
Tselentis et al. (1996)	38.83	20.62	16
Haslinger et al. (1999)	38.84	20.60	13

Table 3

Source parameters of the four retrieved subevents. It is the best-DC part of the DC-constrained moment tensor. Position refers to the trial numbers 1-18 of Fig. 2. Time is relative with respect to the hypocentral time. The variance reduction is denoted *varred*. Highlighted rows correspond to the 5-station solution, while the other rows are for the 4-station reduced data sets (created by successively omitting one station, as indicated in the last column). The reduced data set provide the uncertainty estimate. See also Figs. 5 and 7.

Moment (10^{18}Nm)	Strike (deg.)	Dip (deg.)	Rake (deg.)	*Varred* (x100) (%)	Omitted station
Subevent 1: position 4, time 2 sec					
.47	**17**	**88**	**-177**	**29**	**none**
.54	15	86	-178	33	JAN
.48	20	87	-172	29	EVR
.55	23	86	-178	37	RLS
.50	12	86	-178	34	KEK
.32	198	75	-168	15	SER
Subevent 2: position 12, time 16 sec					
.49	**24**	**74**	**164**	**54**	**none**
.46	22	70	161	54	JAN
.57	27	70	162	60	EVR
.52	25	75	167	57	RLS
.46	21	81	168	60	KEK
.44	26	72	163	42	SER
Subevent 3: position 7, time 5 sec					
.23	**5**	**78**	**-159**	**61**	**none**
.25	8	80	-162	62	JAN
.23	1	82	-146	66	EVR
.25	9	76	-157	65	RLS
.21	7	58	175	66	KEK
.20	360	84	-162	48	SER
Subevent 4: position 7, time 26 sec					
.19	**158**	**89**	**103**	**66**	**none**
.29	133	78	118	70	JAN
.18	145	67	143	68	EVR
.19	176	88	91	70	RLS
.17	325	85	-86	70	KEK
.21	341	89	-105	54	SER

Figure 1. Western Greece, major faults, and seismic stations. Hellenic subduction (line with teeth), the Cephalonia transform fault (arrows) and the continental collision (line with dots) are shown. The PATNET short-period stations used in location are denoted by triangles. The broad-band stations used in the waveform inversion are denoted by squares.

Figure 2. Mainshock (star), aftershocks (circles), trial source positions 1-18 (diamonds), and the resulting four subevents. Shown are the focal mechanisms corresponding to the complete 5-station data set (Table 3). The question mark indicates that subevent 4 is the least certain, in terms of the uncertainty estimate of Figs. 5 and 7. LFS and CFS are geological names of the faults mentioned in the text.

Figure 3a. A 2D-correlation plot to find position and time of the 1st subevent. Note a discontinuity between the trial positions 9 and 10, which are separated 20 km from each other.

Figure 3b. A 2D-correlation plot to find position and time of the 2nd subevent. Note a discontinuity between the trial positions 9 and 10, which are separated 20 km from each other.

Figure 4a. Station SER. Records (top) and synthetics (bottom) for subevent 1 (crosses), and for summed subevents 1+2 (solid line).

Figure 4b. Station JAN. Records (top) and synthetics (bottom) for subevent 1 (crosses), and for summed subevents 1+2 (solid line).

Figure 5. The uncertainty analysis for subevent 1 (top) and subevent 2 (bottom). In the top panel, the observed first-motion polarities are also shown. The highlighted solution is for the complete 5-station data set, while the others are for the reduced 4-station sets.

Figure 6. The preliminary uncertainty analysis for subevent 3 (top) and subevent 4 (bottom). The solution is unstable mainly due to variation of the subevent source position and time.

Figure 7. The final uncertainty analysis for subevent 3 (top) and subevent 4 (bottom). The solution was artificially stabilized by keeping the subevent positions and time fixed at their values obtained with the full 5-station data set.

Figure 8. Observed (top) and synthetic (bottom) band-passed velocity waveforms for summed subevents 1 to 4. The peak values (m/sec) are shown above the station codes. The whole family of synthetics is shown to reflect the uncertainty, as estimated by means of reduced (4-station) data sets. The synthetic data corresponding to the 5-station solution are shown by the thicker line. The three panels (a,b,c) refer to the NS, EW and Z component, as indicated.

Figure 9a. Station SER. Records (top) and synthetics (bottom) for the sum of all four subevents (crosses), and for the subevents 1+2 only (solid line).

Figure 9b. Station JAN. Records (top) and synthetics (bottom) for the sum of all four subevents (crosses), and for the subevents 1+2 only (solid line).

Electronic Supplement
(at http://seis30.karlov.mff.cuni.cz/special/bssa_final)

- All figures of this paper in color version.

- Three additional figures comparing the aftershock location in all three crustal models of Table 2: **`Novotný.jpg, tselentis.jpg, haslinger.jpg`**. The names of the **`jpg`** files correspond to the first-author names of the models.

- An animated 3D demonstration of the aftershock distribution (the double-difference relocation in model by Tselentis et al., 1996) as seen when observer is "moving" around the focal region: **`lefkada.mpeg`**. To see the **`mpeg`** file using the Windows Media Player, a free de-coding software can be used, for example the ’codec’ packages available from http://www.k-litecodecpack.com.

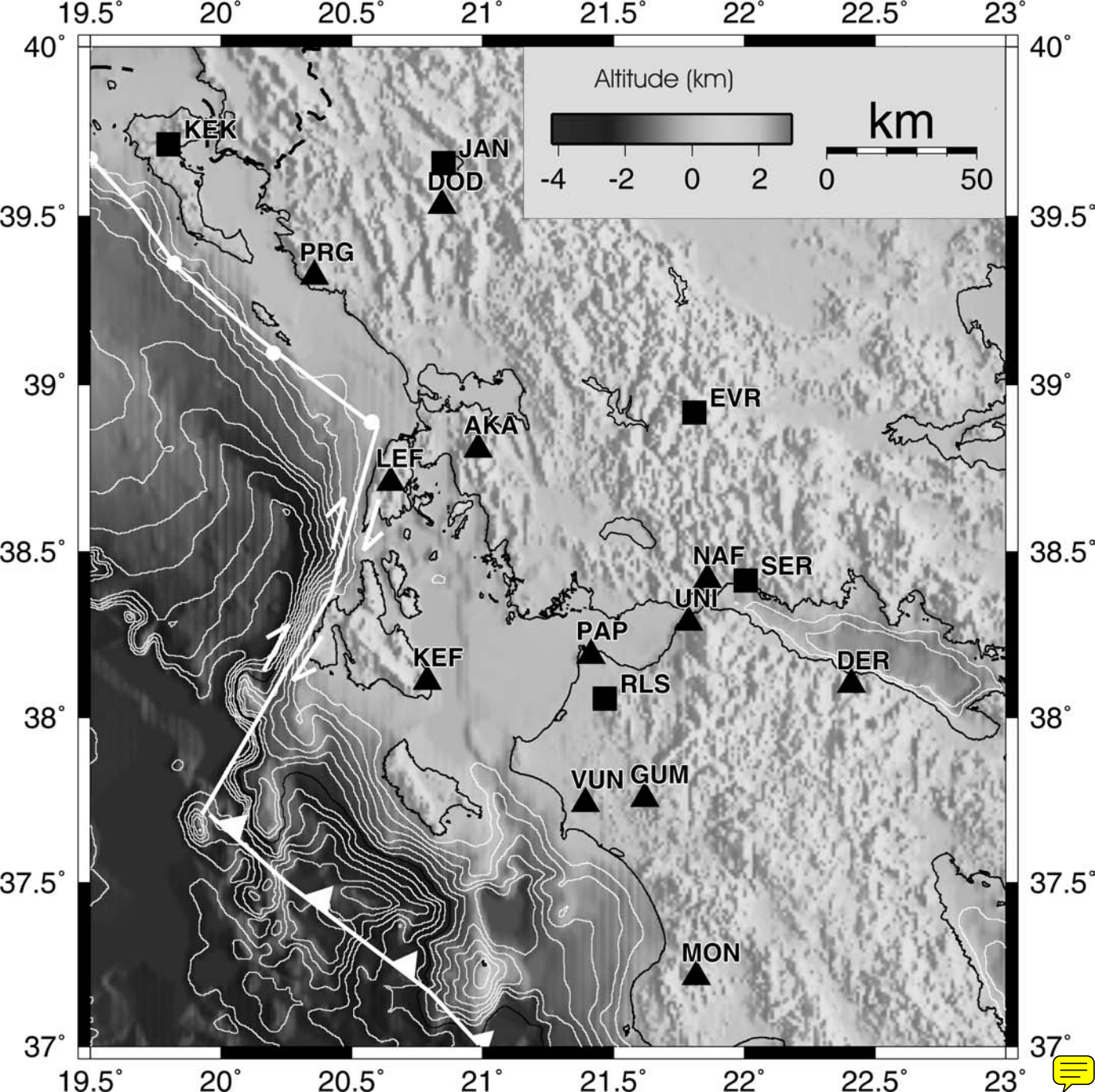
Altitude (km)
-4
-2
0
2
km
0
50
KEK
JAN
DOD
PRG
EVR
AKA
LEF
NAF
SER
UNI
PAP
KEF
DER
RLS
VUN
GUM
MON
19.5°
20°
20.5°
21°
21.5°
22°
22.5°
23°
40°
39.5°
39°
38.5°
38°
37.5°
37°

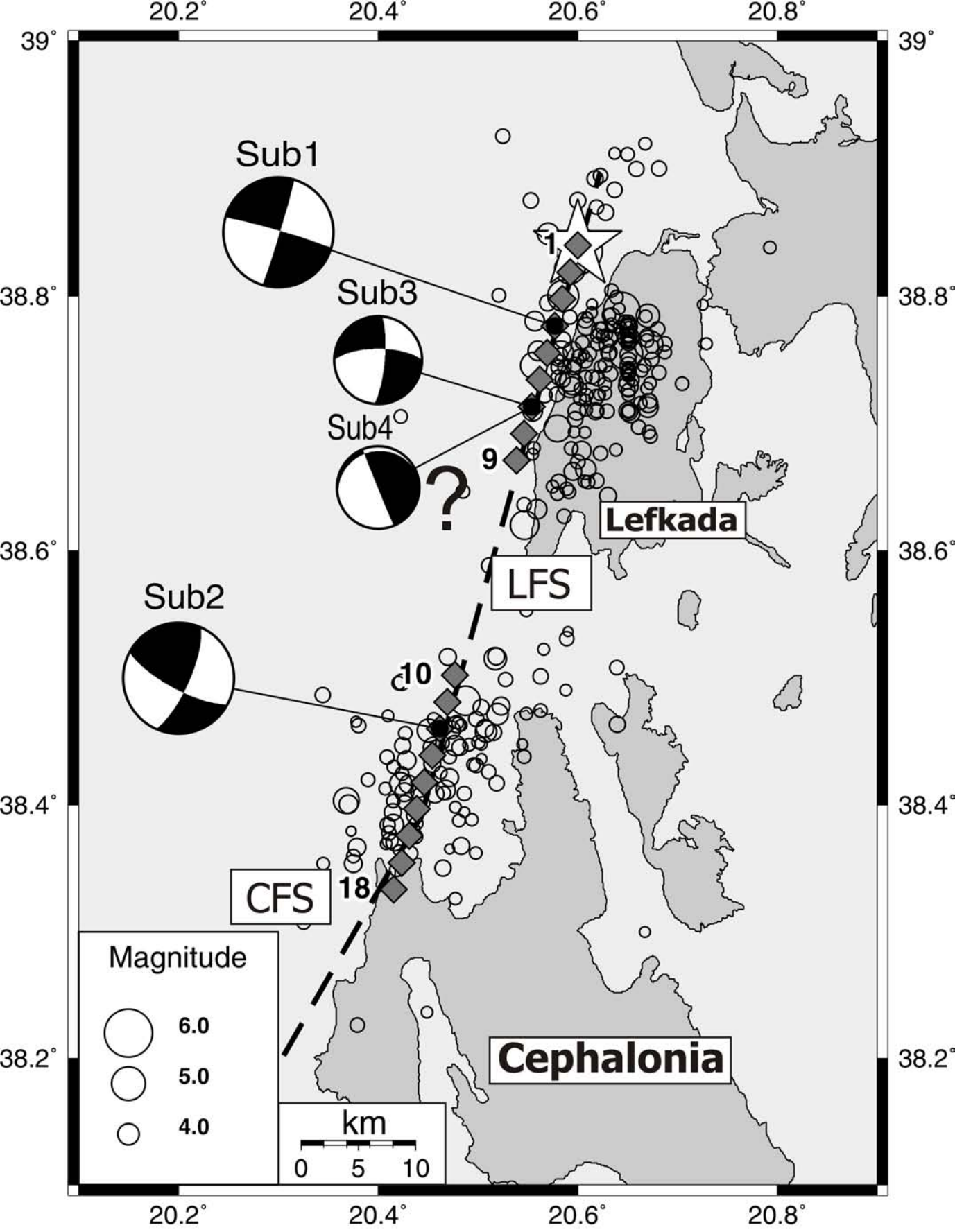
20.2°
20.4°
20.6°
20.8°
39°
38.8°
38.6°
38.4°
38.2°
Sub1
Sub3
Sub4
Sub2
1
9
10
18
?
LFS
CFS
Lefkada
Cephalonia
Magnitude
6.0
5.0
4.0
km
0 5 10

Fig. 2

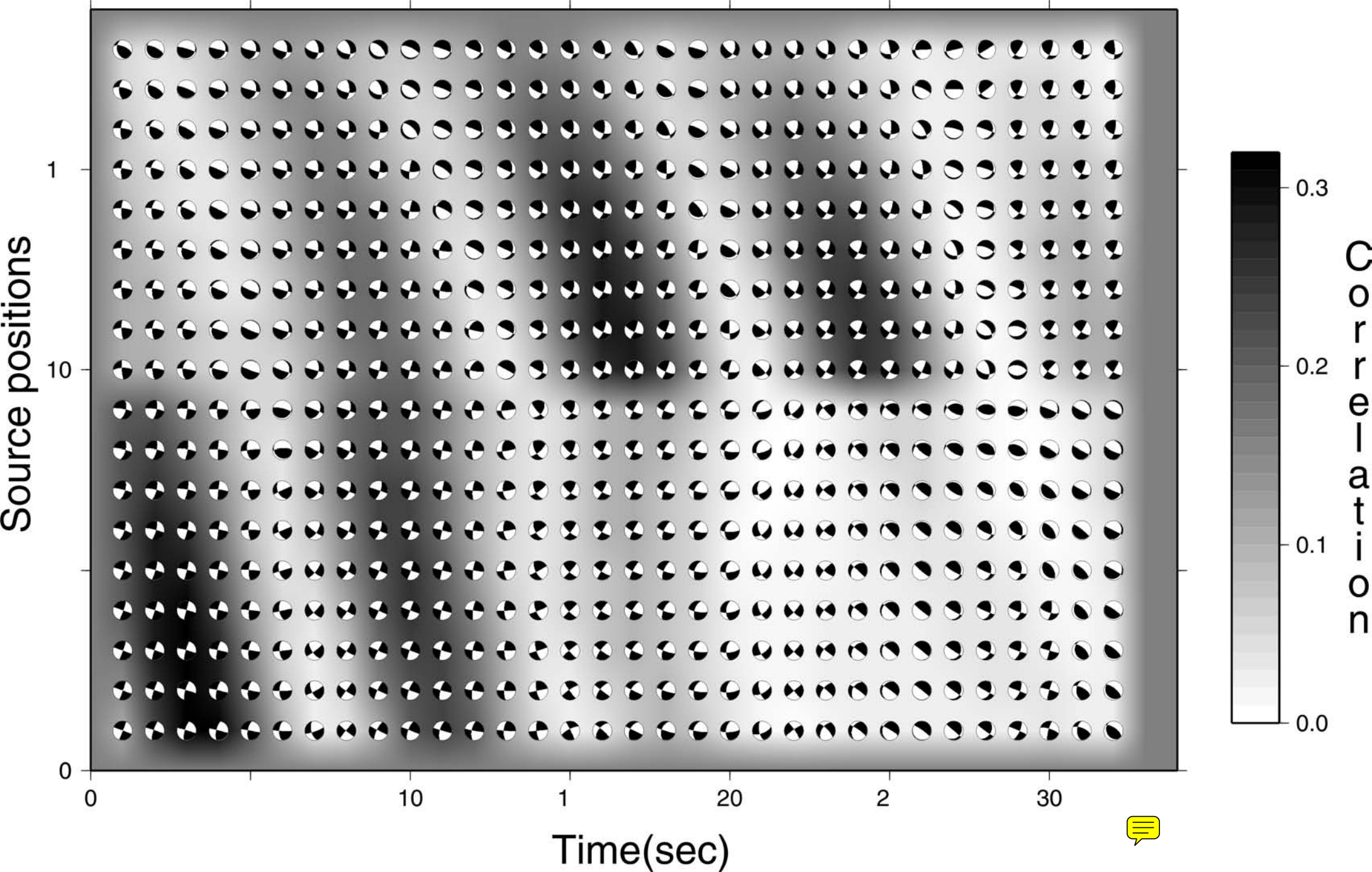
Source positions
1
10
0
0
10
1
20
2
30
Time(sec)
0.3
0.2
0.1
0.0
Correlation

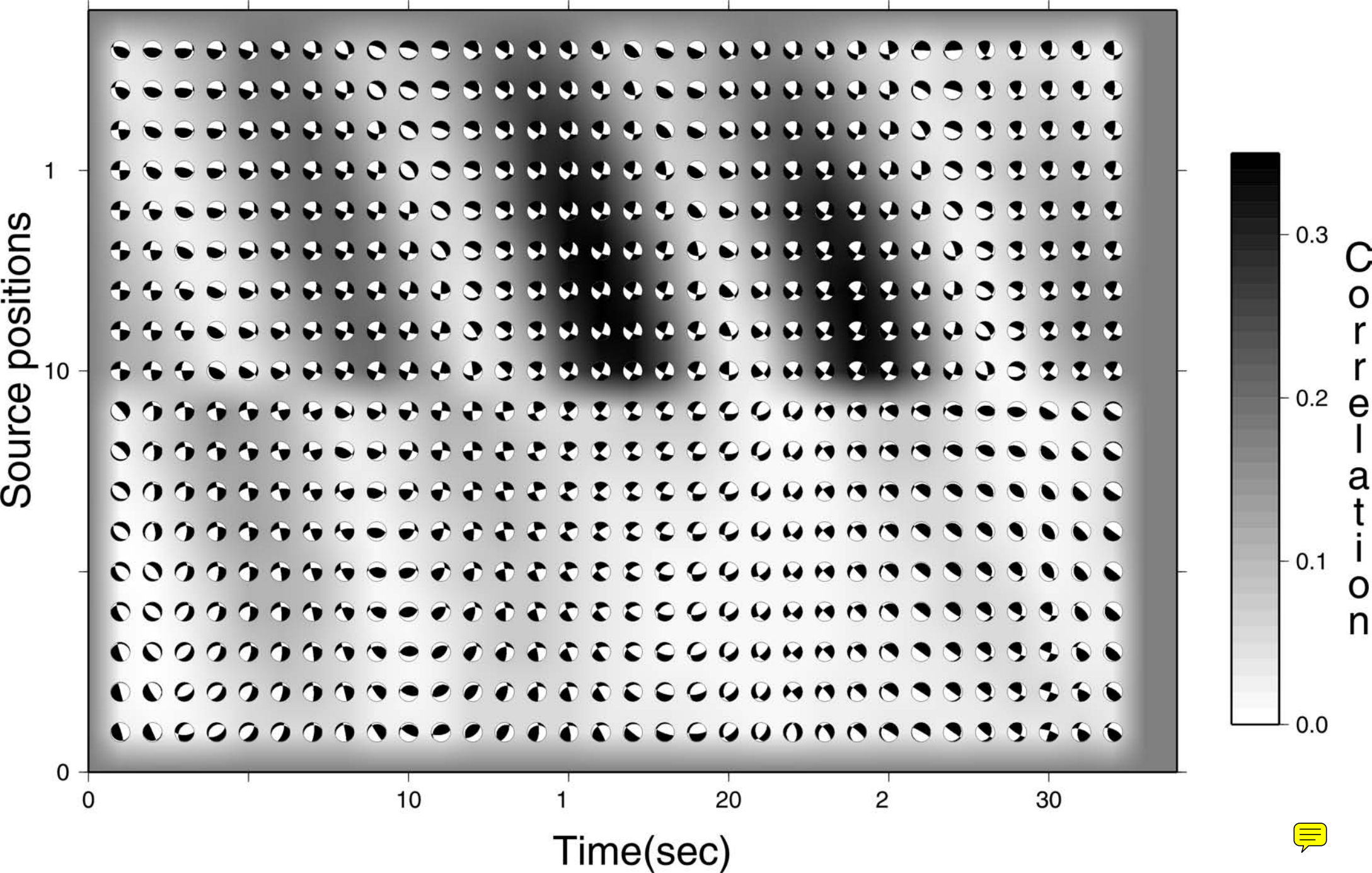
Source positions
1
10
0
0
10
1
20
2
30
Time(sec)
0.3
0.2
0.1
0.0
Correlation

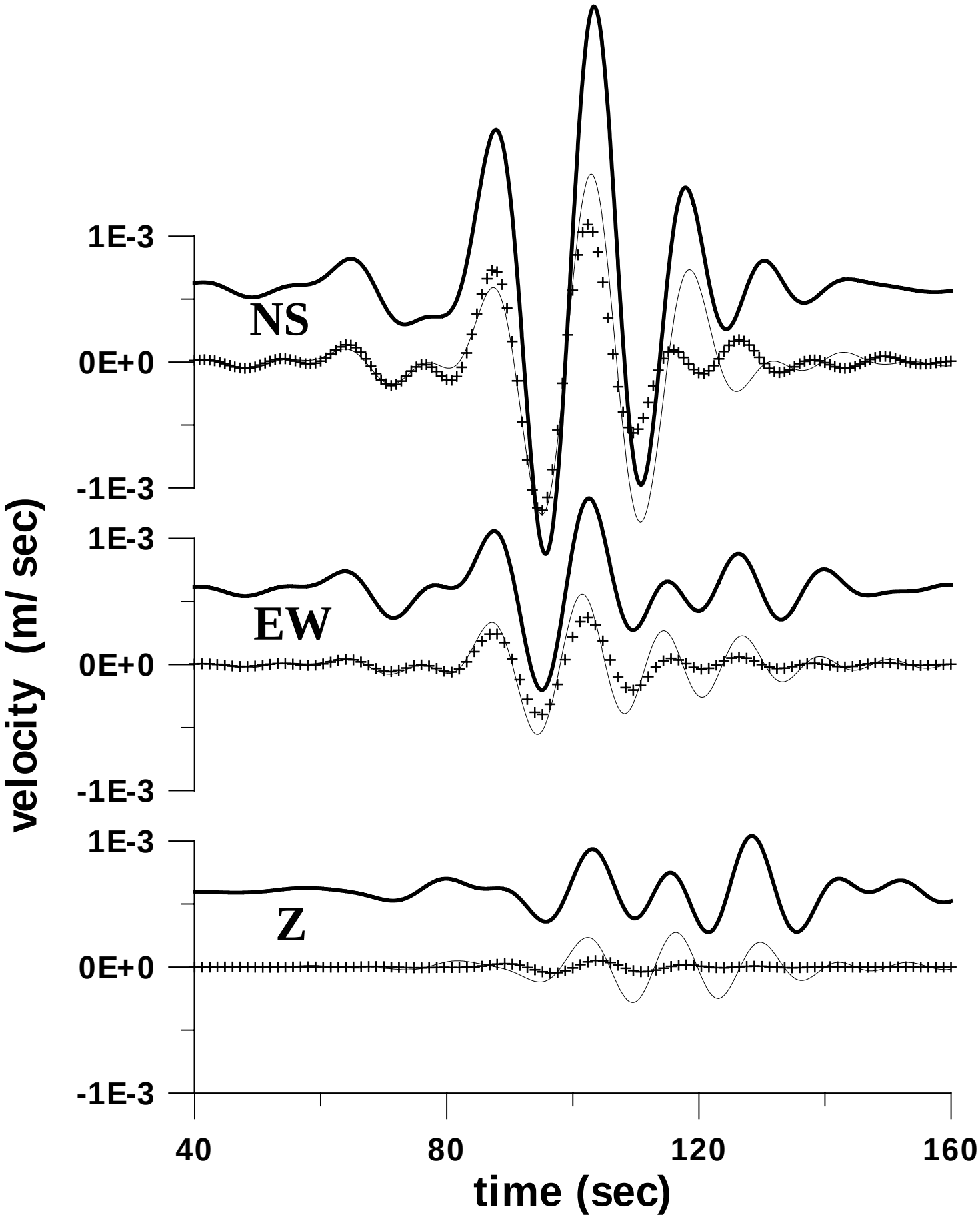
1E-3
0E+0
-1E-3
NS
1E-3
0E+0
-1E-3
EW
1E-3
0E+0
-1E-3
Z
velocity (m/ sec)
40
80
120
160
time (sec)

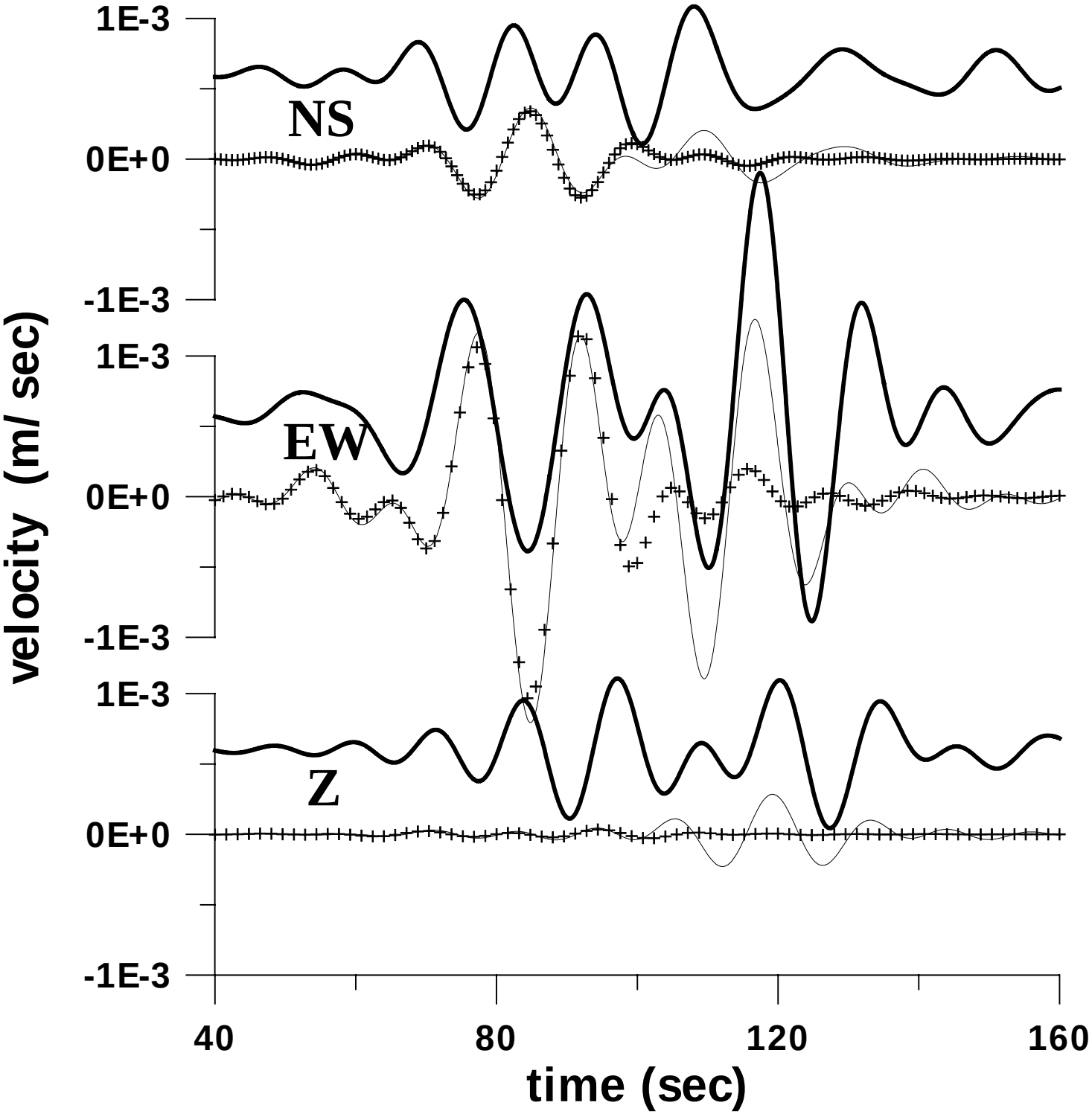
1E-3
0E+0
-1E-3
NS
1E-3
0E+0
-1E-3
EW
1E-3
0E+0
-1E-3
Z
velocity (m/ sec)
40
80
120
160
time (sec)

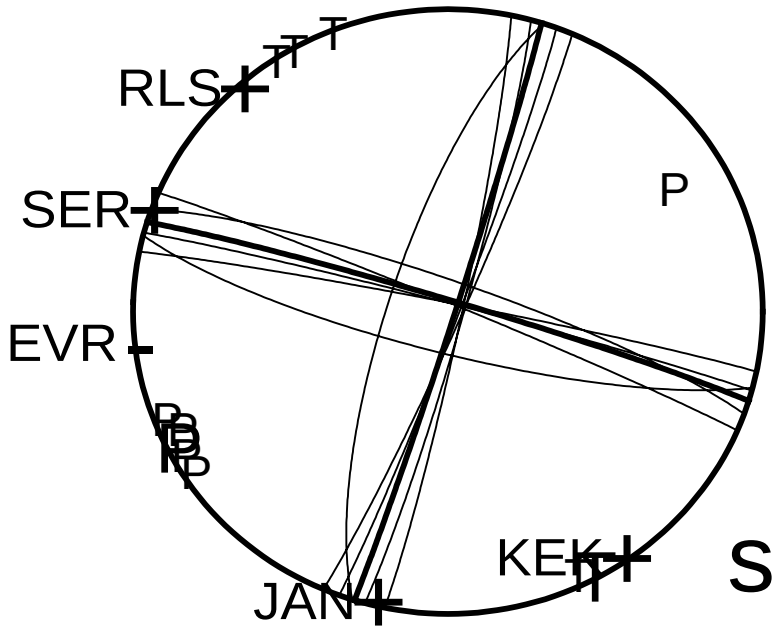

sub 1

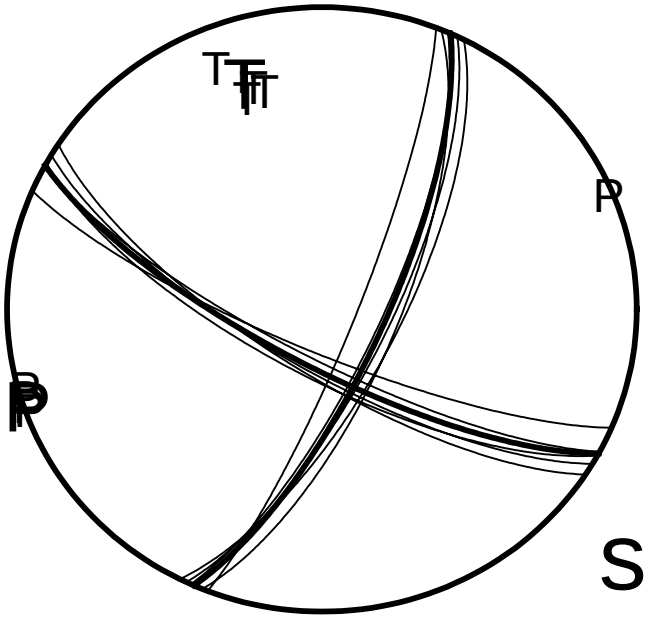

sub 2

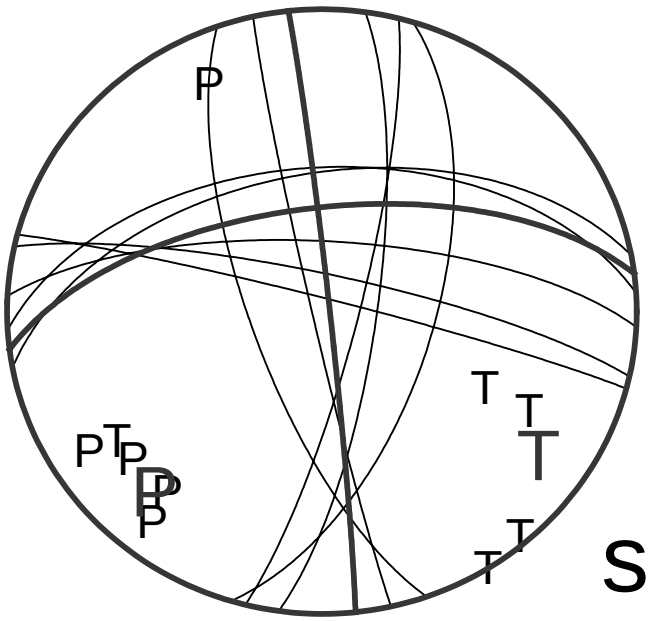

sub 3

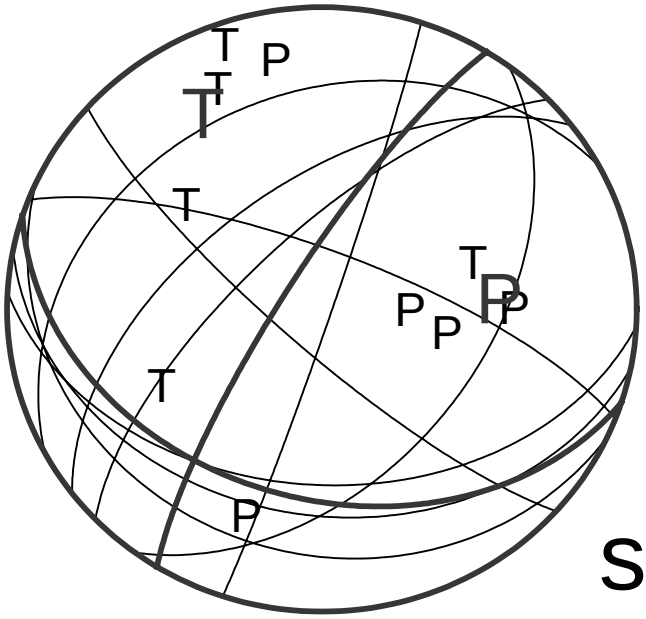

sub 4

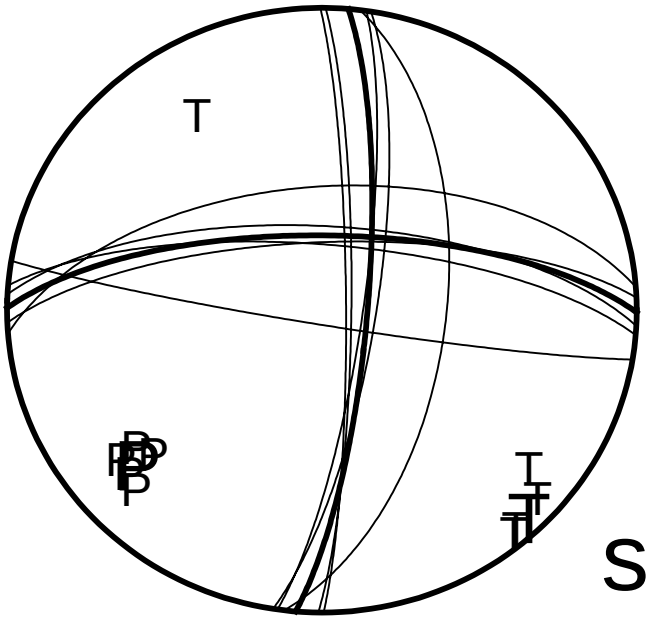

sub 3

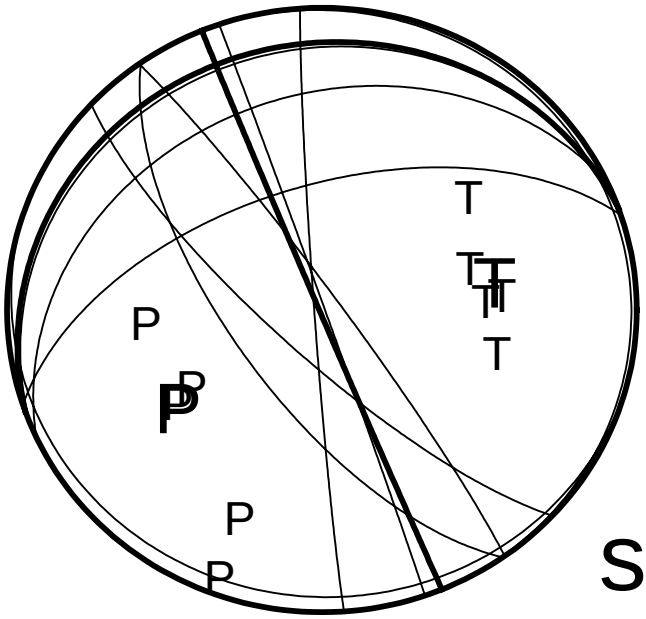

sub 4

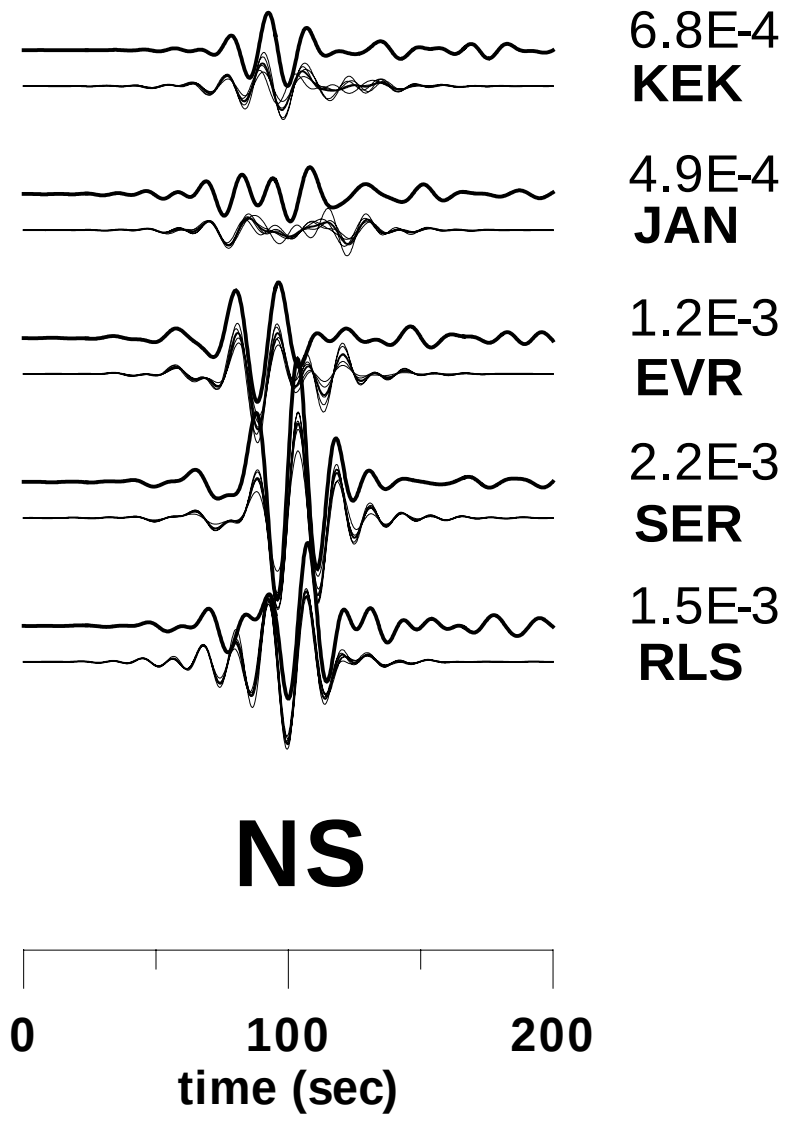
6.8E-4
KEK
4.9E-4
JAN
1.2E-3
EVR
2.2E-3
SER
1.5E-3
RLS
NS
0
100
200
time (sec)

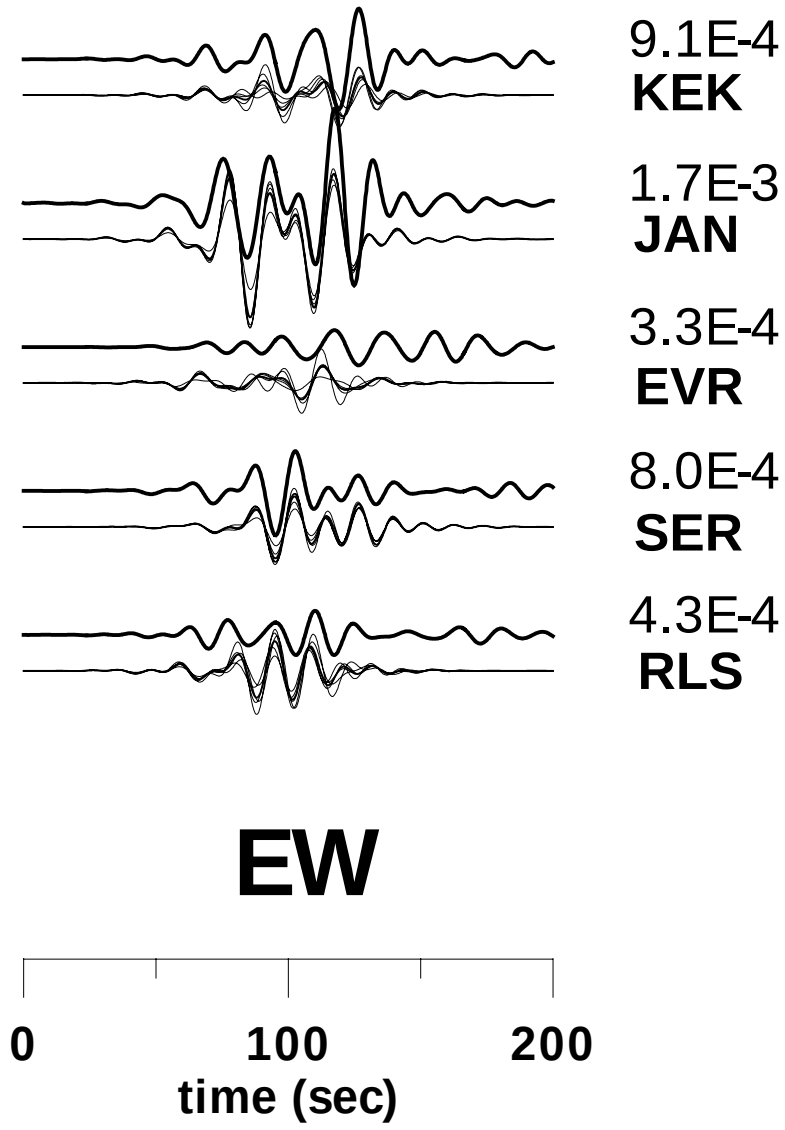
9.1E-4
KEK
1.7E-3
JAN
3.3E-4
EVR
8.0E-4
SER
4.3E-4
RLS
EW
0
100
200
time (sec)

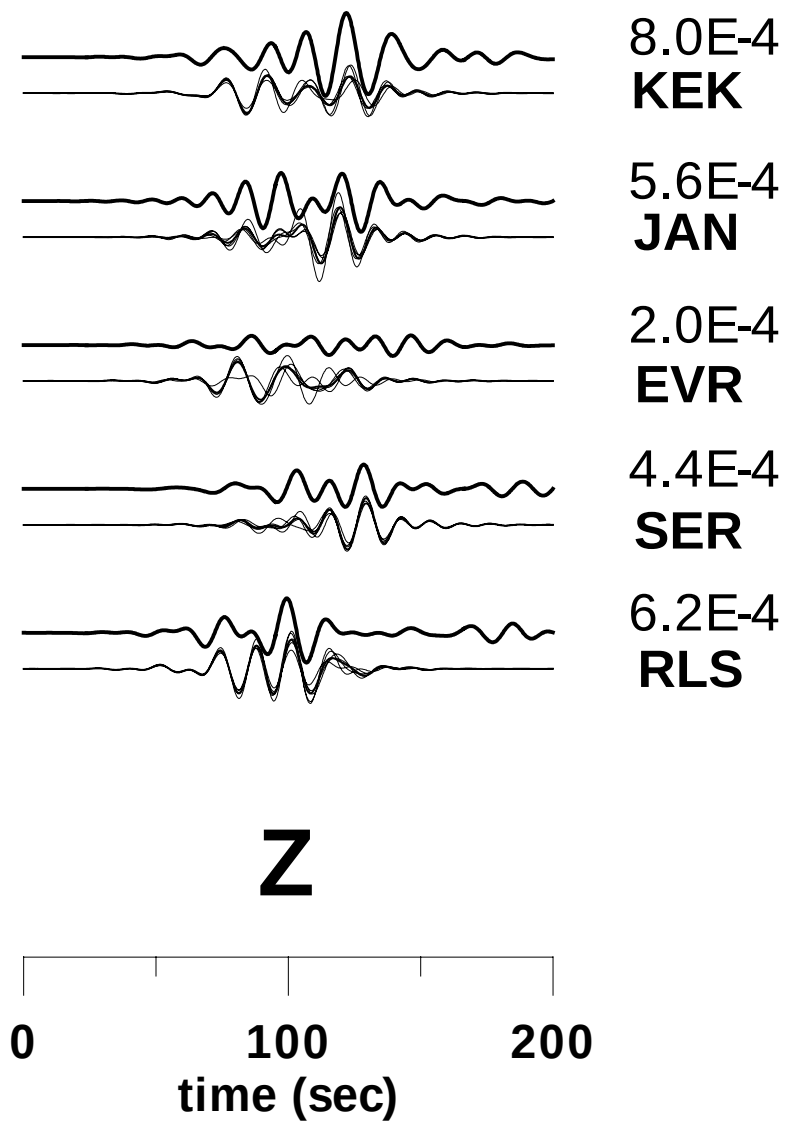
8.0E-4
KEK
5.6E-4
JAN
2.0E-4
EVR
4.4E-4
SER
6.2E-4
RLS
Z
0
100
200
time (sec)

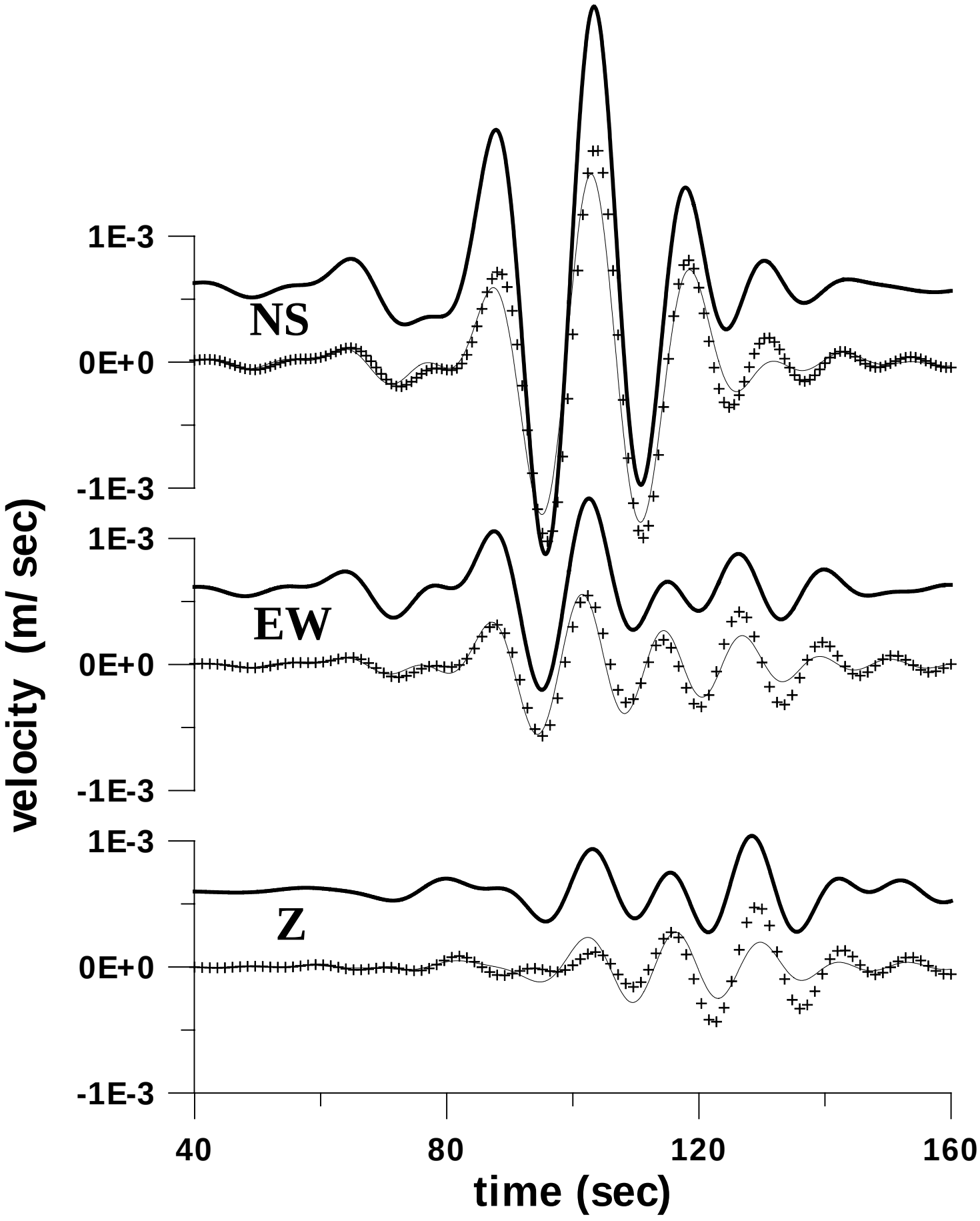
1E-3
0E+0
-1E-3
NS
1E-3
0E+0
-1E-3
EW
1E-3
0E+0
-1E-3
Z
velocity (m/ sec)
40
80
120
160
time (sec)

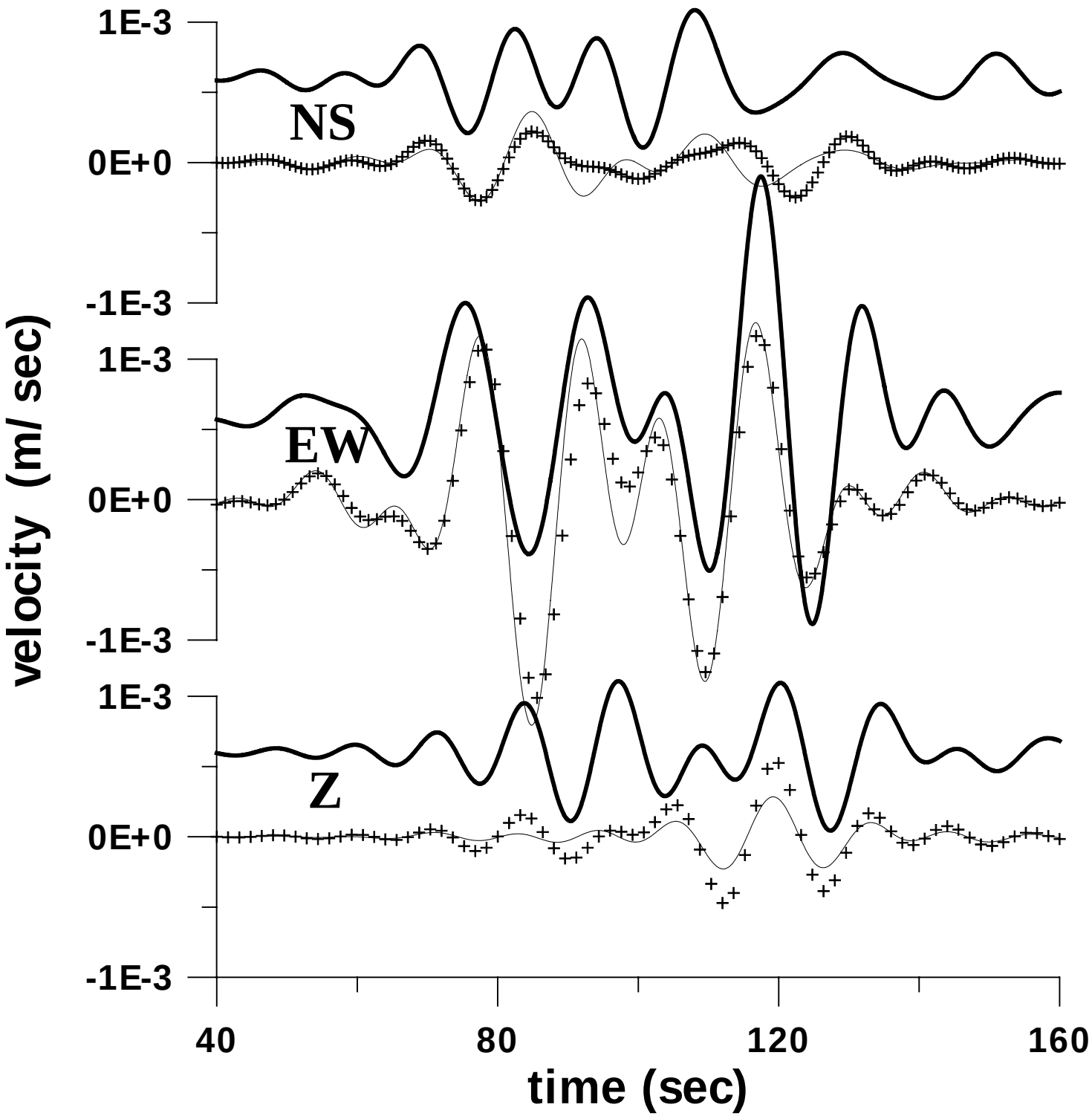
1E-3
0E+0
-1E-3
NS
1E-3
0E+0
-1E-3
EW
1E-3
0E+0
-1E-3
Z
velocity (m/ sec)
40
80
120
160
time (sec)